Science and Technology Indonesia
e-ISSN:2580-4391 *p*-ISSN:2580-4405
Vol. 9, No. 4, October 2024

Research Paper

Synthesis and Characterization of Ni(II) Schiff Base Complex as a Precursor for NiO Nanoparticles and an Investigation of Their Corrosion Inhibition

Shahad Qasim Raji[1], Ali Taleb Bader[1*]

[1]*Department of Chemistry, College of Science for Women, University of Babylon, Hilla, 51001, Iraq*
***Corresponding author**: wsc.ali.taleb@uobabylon.edu.iq*

Abstract
This study first aimed to synthesize and characterize a $[Ni(C_{14}H_{13}NO_2)(OAC)_2(H_2O)_2]$ via the preparation of a ligand, coordination with Ni(II) ions, and full characterization, such as "FTIR, ^{1}H- and ^{13}C-NMR, UV-Visible spectroscopy; and ESI-mass spectrometry" The Nickel complex was then used as a precursor to prepared NiO Nps by calcination at 450°C. The phase purity, crystalline structure, and morphological characterizes of the NiO nanoparticles were investigated via X-ray diffraction (XRD), FESEM, and FTIR spectroscopy, revealing them to be cubic system with an average crystalline is 26 nm. The preparation technique is facile, cost-effective, and rapid and suitable for generating NiO nanoparticles for use in industrial processes. Further, the corrosion inhibition effectiveness of all synthesized compounds on mild steel in 1 M HCl was evaluated. Their inhibition efficiencies were determined via potentiodynamic polarization studies, revealing the highest inhibition efficiency for the NiO nanoparticles compared to the Nickel complex and free a ligand.

Keywords
Schiff Base, Nickel Complex, NiO NPs, Corrosion Inhibition

Received: 6 May 2024, Accepted: 5 August 2024
https://doi.org/10.26554/sti.2024.9.4.914-928

1. INTRODUCTION

In 1864, Hugo Schiff coined the term “Schiff base”(Raczuk et al., 2022) which has remained in use to this day". Schiff bases started gaining attention in the field of coordination chemistry almost a century ago and have remained notably important as ligands (Boulechfar et al., 2023). Schiff base ligands are indeed an important class of compounds in coordination and organometallic chemistry. Schiff bases can form complexes with various transition metals, including copper, nickel, cobalt, and iron. The ligand’s imine nitrogen and other donors can coordinate to the metal center, resulting in chelates that are often very stable. The choice of ligands could electronically tune the metal center’s properties and affect the complex’s reactivity and properties (Devi et al., 2022; Rakhtshah, 2022). For example, Nickel complex have been investigated for the prepared of NiO Nps via calcination (Bader et al., 2024; Prabhakar et al., 2024). This method involves heating the precursor compound to break it down into NiO nanoparticles and is advantageous due to its simplicity, significantly low costs, and yield of high-purity products; it, therefore, presents a very valuable and simple approach for industrial applications (Nassar et al., 2017; Öz et al., 2022; Parsaee et al., 2016; Prabhakar et al., 2024). An example includes NiO nanoparticles with a slightly wide bandgap of 3.6 eV (Ramachandran et al., 2020). Mild steel is applied in many cases and is susceptible to corrosion, notably in an acidic environment.

Hydrochloric acid (HCl) is employed as acidic solution in pickling applications and used to strip mild steel surfaces of, for example, stains, corrosion, rust, inorganic compounds, etc. After conducting a literature review on this issue, we noted that a range of organic inhibiter types was constructed to reduce the corrosion and vulnerability of plain carbon steel materials in acidic media (Afshari et al., 2023; Ansari et al., 2014; Wadhwani et al., 2015). Similarly, the large size and strong coordination characteristics of transition metal complexes of Schiff base ligands imply that such materials may show optimal performance among all considered systems and highlight the beneficial synergistic effect of metal–organic hybrids (Mishra et al., 2015).

Scholars have observed that metal–ligand complexes are significantly more effective in corrosion inhibition than uncomplexed ligands (Kashyap et al., 2018; Mofidabadi et al., 2024). Recently, nanotechnology has attracted considerable attention for its broad applicability in materials science, including corrosion science, and its use in elucidating their properties and applications. “Nanoparticles, ranging in size from 1 to 100

nm", can be employed in corrosion science (Atta et al., 2013), an area where various metal and metal oxide nanoparticles have been studied. This study examines the corrosion inhibition performance of NiO nanoparticles, highlighting their novel application in this context. Specifically, the Schiff base complex of nickel(II) with 2-[(4-methoxybenzylidene)amino]phenol (MBZ) was assessed for its ability to inhibit the corrosion of carbon steel in 1 M HCl. The bidentate ligand (MBZ) in the metal–ligand complex were synthesized and was successful in coordinating the metal ions through O and N, as revealed by "ultraviolet-visible (UV-Vis), "Fourier transform infrared (FTIR), and proton and carbon-13 nuclear magnetic resonance (^{1}H- and ^{13}C-NMR) spectroscopy". The calcination of the complex to produce the NiO Nps was then carried out. The interest in this was essential to promote the benefits of the technique. "Finally, FTIR spectroscopy, X-ray diffraction (XRD), energy-dispersive X-ray (EDX) spectroscopy", and scanning electron microscopy (SEM) were used to characterize the NiO NPs.

2. EXPERIMENTAL SECTION

2.1 Materials

These included anisaldehyde (Merck, Germany); 2-aminophenol (Merck); nickel acetate tetrahydrate, or $Ni(CH_3COOH)_2.4H_2O$ (BDH, England); and CH_3CN (0.1% formic acid) : H_2O.

2.2 Instrumentation

The Stuart digital melting point apparatus is favored for its speed and precision, SMP30, was employed for the melting point determination. FTIR spectroscopic analysis was performed on the compounds (molecular structure and functional groups) using a Shimadzu FTIR spectrophotometer (Broker model), operating in transmission mode over a range of 4000–400 cm^{-1}. In the FTIR analysis, the samples were combined with KBr into a suspension and pressed into disks, which was important in the chemical identification of the materials. UV-Vis spectra were recorded on a Shimadzu UV-Vis spectrophotometer (model 1700) to obtain electronic transitions of the molecular compounds. The molecular structure of the ligand was analyzed using ^{1}H NMR and ^{13}C NMR spectra, recorded with a Bruker DMX-400 spectrometer operating at 400 MHz. XRD was carried out using a Philips X'pert diffractometer with Cu Kα radiation as a monochromatic source; SEM with gold coatings was used to characterize the sample and generate the XRD patterns. In the liquid chromatography (LC)-electrospray ionization (ESI)-mass spectrometry (MS) analysis, a column temperature of 30°C and flow rate of 0.4 ml/min were applied using the Shimadzu UFLC LC-AD20 system (Shimadzu, Japan) connected to a 3200 QTRAP mass spectrometer.

2.3 Synthesis Procedures

2.3.1 Synthesis of o-[(p-methoxybenzylidene)amino]phenol (MBZ)

A one-pot synthesis, as shown in Figure 1, was employed to prepare the Schiff base ligand according to procedures given in the literature (Sharma et al., 2022). Here, anisaldehyde (2.5 g, 0.0183 mol) was first mixed with an alcoholic solution of 2-aminophenol (1.96 g, 0.0183 mol). After refluxing for 6 hours, the mixture was colloing, resulting in the formation of brown crystals as reaction products.

2.3.2 Synthesis of Nickel Complex

A hot suspension of the Ligand (MBZ; 0.5 g, 0.002 mol) in absolute ethanol (20 ml) was first prepared, and $Ni(CH_3COO)_2.4H_2O$ (0.54 g, 0.002 mol) in ethanol (10 ml) was then added. The deep green solution was stirred and refluxed for 4 h, and the resultant solid product was filtered, washed with cold methanol, and dried in a rotary evaporator to yield a yellow solid product is illustrated in Figure 1 (Gönül et al., 2018).

2.3.3 Synthesis of NiO Nps

In Figure 1,the a $[Ni(C_{14}H_{13}NO_2)(OAC)_2(H_2O)_2]$ was synthesized and used as a precursor for NiO Nps synthesis. To this end, the green precipitate of this compound was placed in a porcelain flask at a temperature above 500°C for 4 hours (Bader et al., 2024).

2.4 Characterizations

The (MBZ) ligand and Nickel complex were characterized by UV-Vis, FTIR, atomic absorption, and ^{1}H- and ^{13}C-NMR spectroscopy; ESI-MS; and XRD. The melting point and magnetic susceptibility were also evaluated. The NiO NPs were evaluated via UV-Vis, FTIR, and EDX spectroscopy; XRD; and field emission scanning electron microscopy (FESEM).

2.5 Corrosion Testing for the MBZ (ligand), Ni(II) Schiff Base Complex, and NiO Nanoparticles

The potentiostat unit comprises a host computer, thermostat, magnetic stirrer, potentiostat (EmStat 4s, Palm Sens, Holland), and galvanostat, as shown in Figure 2. The cell has an internal and external beaker (250 mL) and is made from Pyrex. The cell contains three electrodes: a working electrode of carbon steel to determine its potential with the reference electrode; an auxiliary electrode composed of platinum, with a length of 10 cm; and a reference electrode involving a saturated calomel electrode (Hg/Hg_2Cl_2 sat. KCl). The working electrode was immersed in the solution – Schiff base ligand, Ni(II) complex, and NiO NPs – for 15 min to obtain a steady-state open-circuit potential (EOCP) before using the cell for electrochemical measurements in the potential range of ± 200 mV. All tests were carried out at 298 K using a cooling–heating circulating water bath (Boulechfar et al., 2023; Mamudu et al., 2024).

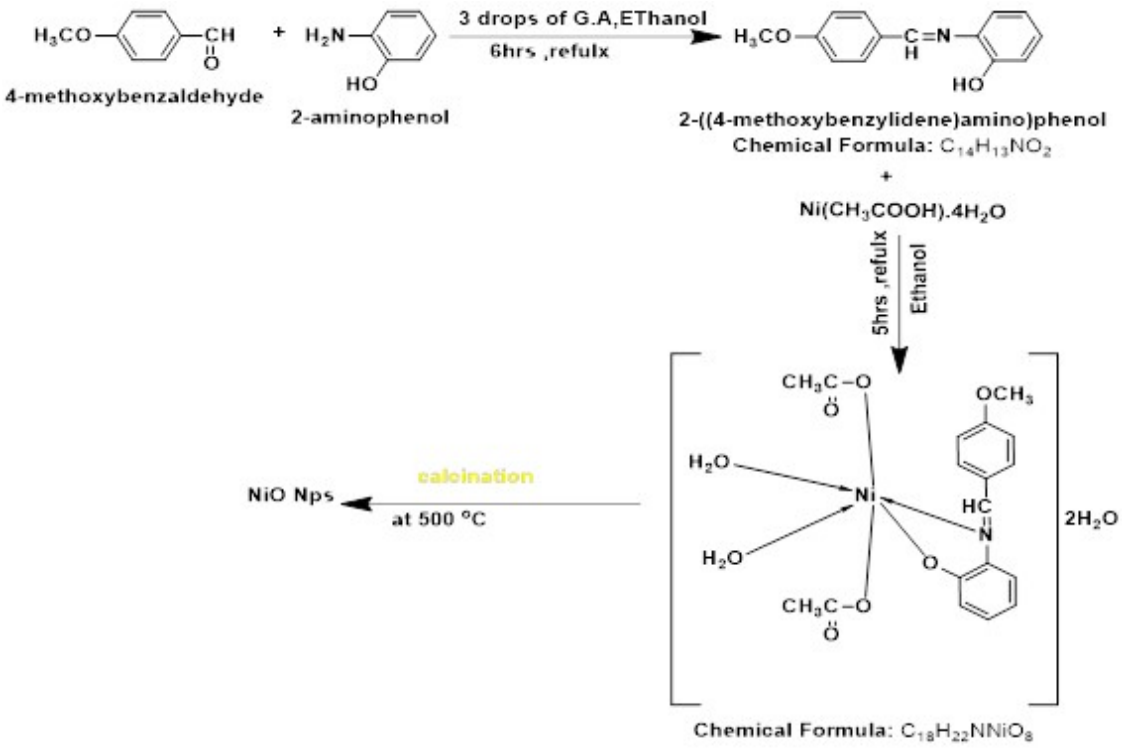

Figure 1. Preparations of the MBZ (ligand), Nickel(II) Complex, and NiO Nanoparticles

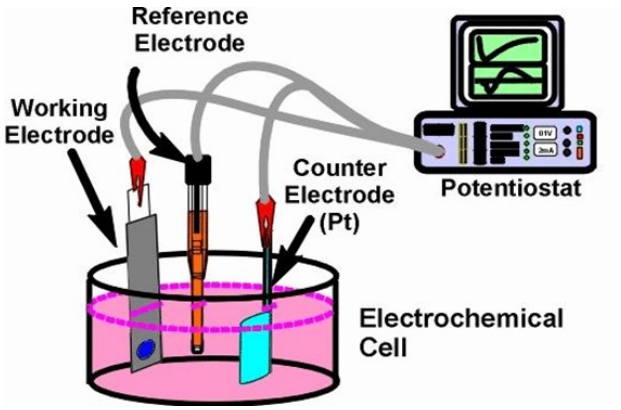

Figure 2. Configuration of the Corrosion Cell and Three-Electrode System

3. RESULTS AND DISCUSSION

3.1 Characterization of the Schiff Base (Ligand), Its Ni(II) Complex, and NiO Nanoparticles

3.1.1 FTIR Spectroscopy of the Ligand (MBZ), Ni(II) Complex, and NiO Nanoparticles

FTIR spectroscopy was used to assign the major vibrational bands of the synthesized compounds. Before analyzing the spectrum of the ligand (L), it is important to examine the major FTIR bands in Table (1) of the most significant components involved in its preparation. The FTIR spectrum of anisaldehyde in Figure 3 exhibits a C=O_{st} at 1687 cm^{-1}; bands due to C=O wiggles at 2840 and 2950 cm^{-1} due to symmetric and asymmetric stretching of the methyl (C−H) group for the carbonyl group, respectively; and three C=C stretching bands at 1597, 1509, and 1430 cm^{-1}, as noted in previous literature (Silverstein et al., 2005) However, the FTIR spectrum of 2-aminophenol also shows two bands at 3350 and 3375 cm^{-1}, corresponding to N−H symmetric and asymmetric stretching, respectively, and a band at 1604 cm^{-1}, assigned to N−H bending (Ahmed and Galtima Lemos, 2021) The FTIR spectrum of the ligand (L) exhibits variations: for the major affinity, it shows a decrease in the energy associated with υNH; the disappearance of a band at (3350, 3375 cm^{-1}) is due to asymmetric and symmetric NH_2 stretches; the band for the C=N imine group at 1633 cm^{-1} confirms the formation of the Schiff base; and the band at 3051 cm^{-1} confirms the formation of υ(O−H). In Figure 4, in the case of the complex, the C=N imine group moves to a lower wavenumber. In the ligand (L), the C=N imine group binds the metal through the N atom. The stretching vibrations of the hydroxyl groups (O−H) shift to higher frequencies or appear as broad vibrations with several peaks and lower energies. There are changes in the conformation of the hydroxyl groups, and the broad vibrations indicate the interactions of the metal ion with the imine N atom and the thiol O atom. The main broad vibrations of the ligand, complex, and NiO NPs are shown in Table 1. As shown in Figure 4, it was confirmed that pure NiO NPs were formed in the absorption band at 450 cm^{-1}.

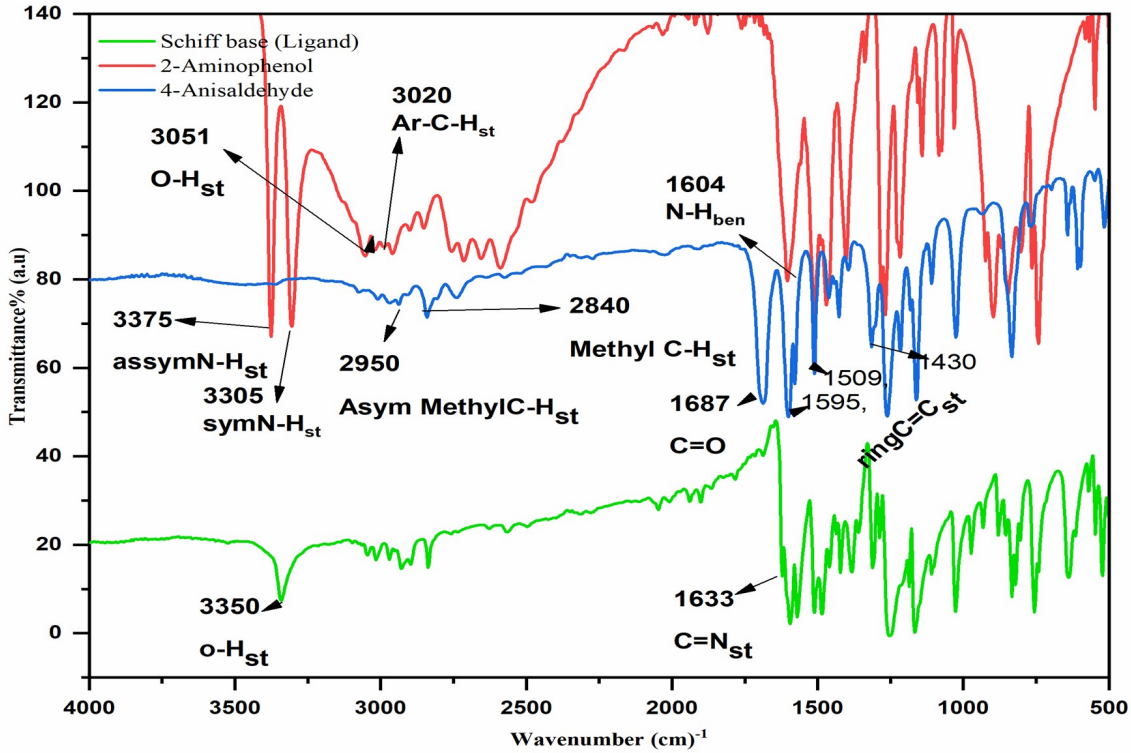

Figure 3. FTIR Spectra of Anisaldehyde, 2-Aminophenol, and the Ligand (Schiff Base)

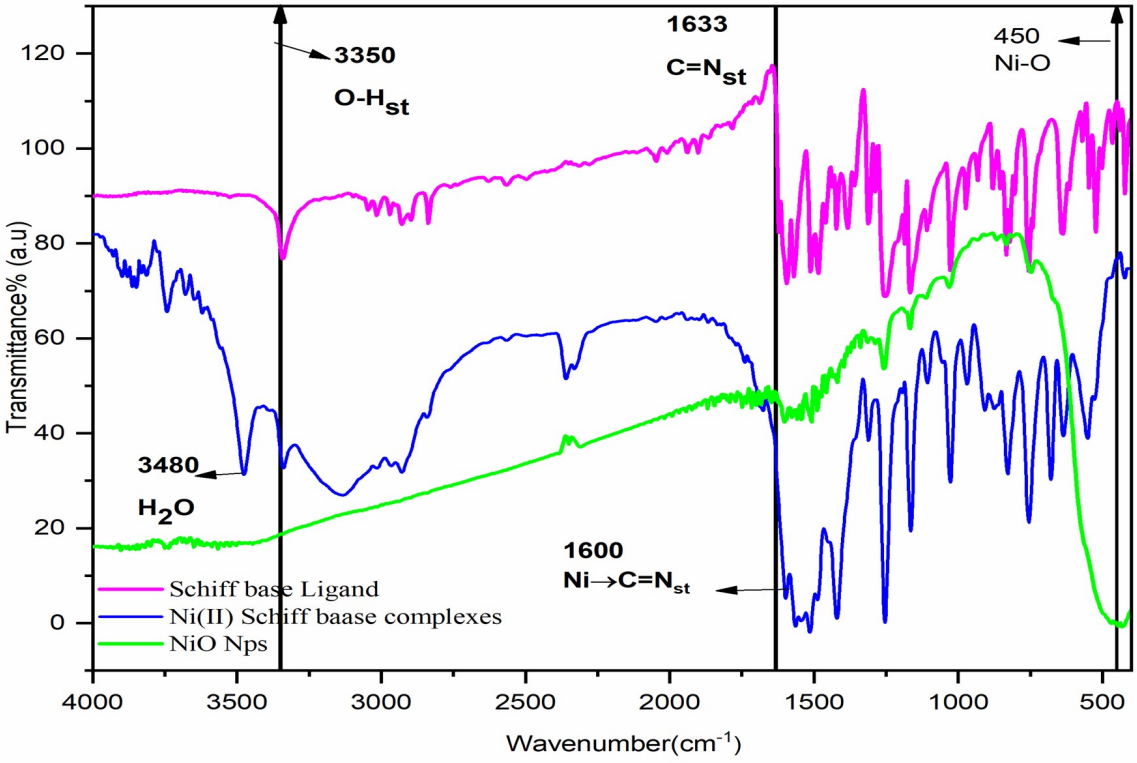

Figure 4. FTIR Spectral Distributions of the Ligand, $[Ni(C_{14}H_{13}NO_2)(OAC)_2(H_2O)_2]$, and NiO (NPs)

Table 1. FTIR Spectral Characterizations of the Precursors (Anisaldehyde and 2-Aminophenol), Ligand, Metal–Ligand Complex, and Metal Oxide Nanoparticles

Compound	υ(C=O) cm^{-1}	$\upsilon(NH_2)$ asym-sym cm^{-1}	υ(CH=N)	υ(O−H) cm^{-1}	υ(C−H) cm^{-1}	υ(M−N) cm^{-1}	υ(M−O) cm^{-1}
Anisaldehyde	1687	—	—	—	2840, 2950	—	—
2-Aminophenol	—	3375-3350	—	—	—	—	—
Schiff Base (Ligand)	—	—	1631	3350	—	—	—
Ni(II) Schiff Base Complex	—	1600	—	—	—	420	458
NiO NPs	—	—	—	—	—	—	450

Table 2. Electronic Spectral Data in Ethanol (Solvent) and Magnetic Moments (B.M.) for L and Its Ni(II) Metal Complex

Compound	Absorption Bands (nm)	Assignments	μ_{eff} B.M. (Cal.)	Metal % (Cal.)	Suggested Geometry
Schiff Base (Ligand)	207	$n \rightarrow \pi*$	—	—	—
	283	$\pi \rightarrow \pi*$			
	345	$n \rightarrow \pi*$			
$[Ni(C_{14}H_{13}NO_2)(OAc)_2(H_2O)_2]$	420	3A2g(F)→3T1g(P)	3.37 (2.88)	11.8 (12.3)	Octahedral
	685	3A2g(F)→3T1g(F)			
	217	MLCT			
	272	MLCT			

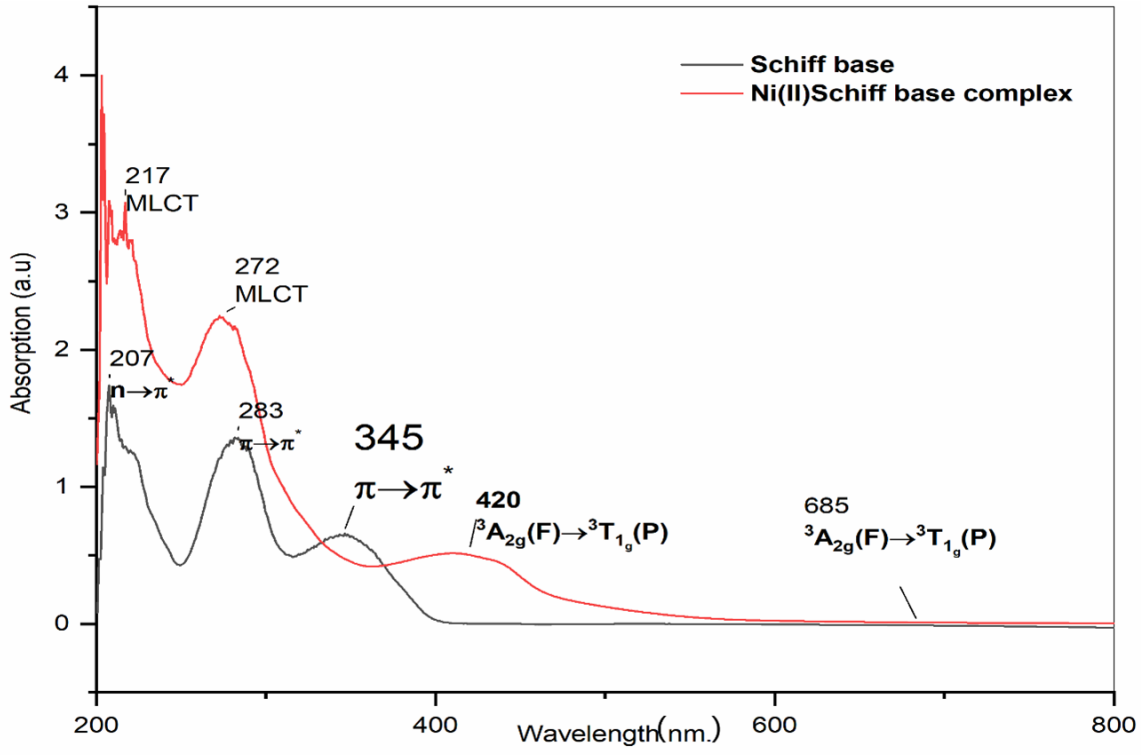

Figure 5. Electronic Spectra of the MBZ (Ligand) and Its Nickel Complex

Table 3. ^{1}H-NMR Characterization of MBZ (ligand)

H/C	Chemical Shift (δ)	Interpretation	Reference
$-\delta$OH	9.8 ppm	Singlet, attributed to phenolic group	(Ezeorah et al., 2022) (Silverstein et al., 2005)
δCH=N	8.9 ppm	Singlet, due to Schiff base group (imine)	(Kargar et al., 2021)
δ(8H)	6.8–8.6 ppm	Observed multiple protons for the aromatic rings	(Platzer et al., 2020)
δ(DMSO)	2.5 ppm	Signal peak attributed to the solvent	(Quevedo, 2020)
$\delta(H_2O)$	3.4 ppm	Due to hydration	(Streicher, 2018)

Table 4. ^{13}C-NMR Data for MBZ (ligand)

C/H	Chemical Shift (δ) / ppm	Characterizations	References
$-CH_3$	56.6	Due to CH_3 of anisaldehyde	(Silverstein et al., 2005)
$C-OCH_3$	164	Due to OCH_3 of anisaldehyde	(Agrawal and Blunden, 2023)
$-CH=N$	160	Observed for imine group	(Atzin-Macedo et al., 2020)
C−OH	151	Due to the phenolic group	(Quevedo, 2020)
(C−aromatic)	δ=114–144	Due to the aromatic carbons	(Silverstein et al., 2005)
δ(DMSO)	40	Due to the solvent	(Khodov et al., 2023)

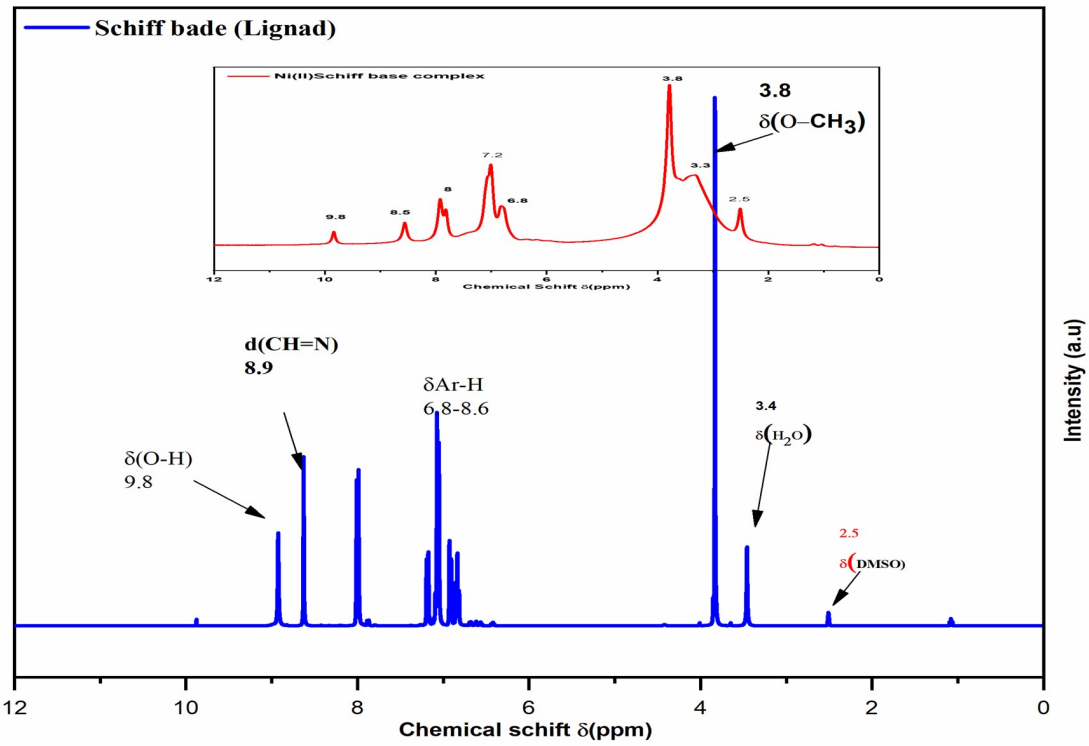

Figure 6. ^{1}H-NMR Spectra of the MBZ (ligand)

3.1.2 Electronic Transitions and Magnetic Susceptibility of the the MBZ (Ligand) and $[Ni(C_{14}H_{13}NO_2)(OAC)_2(H_2O)_2]$

From the transitions shown in Figure 5, three bands were: (35587.19 cm^{-1}, 281 nm), (28901.73 cm^{-1}, 346 nm), and (22675.74 cm^{-1}, 441 nm). These are identified as n→π* and π→π* transitions and are summarized in Table 2. The Schiff base functionality leads to C=N conjugation, broadening the absorption in the visible region as well as two bands at 23809.52 cm^{-1} (420 nm) and 14598.54 cm^{-1} (685 nm) due to 3A2g(F)→3T1g(P) and 3A2g(F)→3T1g(F) transitions (Kargar et al., 2022; Kumar et al., 2023). The measurement of the magnetic properties was also found to be useful in the identification of the complex structure; this might provide some insight, partially or initially, and is one of the methods of providing preliminary though incomplete information (Bain and

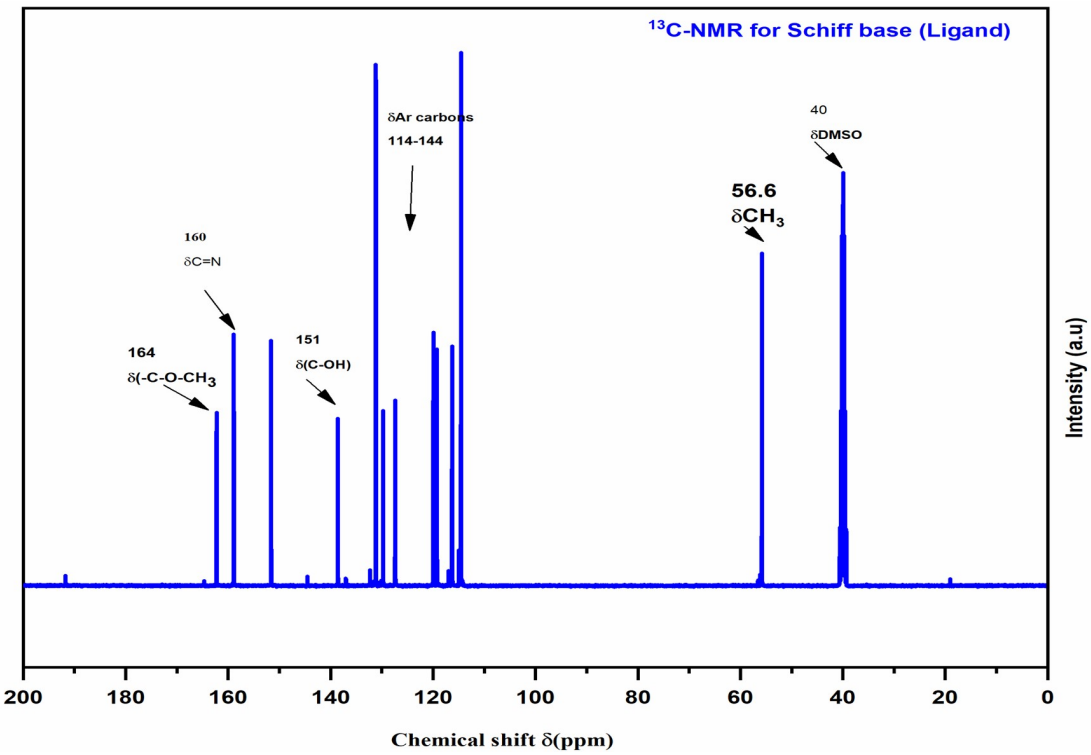

Figure 7. ^{13}C-NMR Spectra of the MBZ (ligand)

Berry, 2008). Quantities of unpaired electrons values in the early transition metals. The effective magnetic spin of two nuclear spin-1/2's in each complex was measured and calculated using only a spin magnetic moment (μs.o), according to Equation 1:

$$\mu_{effect} = 2\sqrt{n(n+1)} \quad (1)$$

The magnetic susceptibility values of the substances were measured by Gouy's, while Pascal's constant was used as a parameter to estimate the diamagnetism correction of different atoms (Bain and Berry, 2008). By applying the effective magnetic moment values, μ_{eff}, the following equation was used:

$$\mu_{eff} = 2.83\sqrt{(\chi MT)} \quad (2)$$

where χM is the magnetic susceptibility, and T is the absolute temperature. The values and findings obtained from Equations 1 and 2 were compared to the actual measured magnetic properties (Table 2). The calculated value of the magnetic moment given by Equation 2 was larger than the value obtained by the spin-only formula because of the orbital contribution to the magnetic moment (Bain and Berry, 2008; Lupascu et al., 2021).

3.2 ^{1}H-NMR Spectroscopy of the MBZ (Ligand) and Its [Ni($C_{14}H_{13}NO_2$)(OAC)$_2$(H_2O)$_2$]

^{1}H-NMR spectroscopy represents an effective approach to investigating the structure of Schiff base compounds by analyzing the behavior of hydrogen nuclei in a magnetic area. The ^{1}H-NMR peaks of the ligand were recorded in DMSO (Figure 6), and Table 3 presents the peak assignments. Similarly, in the case of the nickel complex, paramagnetism results in the transferring of NMR peaks. Because of the presence of unpaired electrons on the steel ion, these spectra also provide approximate data on the coordination environment and electronic shape of the complex (Kareem et al., 2021; Kumar et al., 2023).

3.3 ^{13}C-NMR Spectra of the MBZ (Ligand)

^{13}C-NMR spectroscopy represents another important technique for structural elucidation, particularly in organic chemistry. It shows the location and environment of carbon atoms in a molecule.

The ^{13}C-NMR spectrum of the ligand L is shown in Figure 7. Unlike the case in ^{1}H-NMR spectra, carbon atoms do not typically exhibit significant coupling with neighboring carbons. However, multiplicity (splitting) may still be observed due to coupling with directly bonded hydrogen atoms. The ^{13}C-NMR chemical shifts for the ligand are presented in Table 4.

3.3.1 ESI-Mass Spectral Characterization of the MBZ (ligand) and Its [Ni($C_{14}H_{13}NO_2$)(OAC)$_2$(H_2O)$_2$]

The MS data presented concern the complex with the chemical formula $C_{10}H_{22}NNiO_{10}$ and a molecular weight of 475.10 g/mol. Figure 8 shows the spectrum at various mass-to-charge (m/z) ratios, which are important for identifying and elucidat-

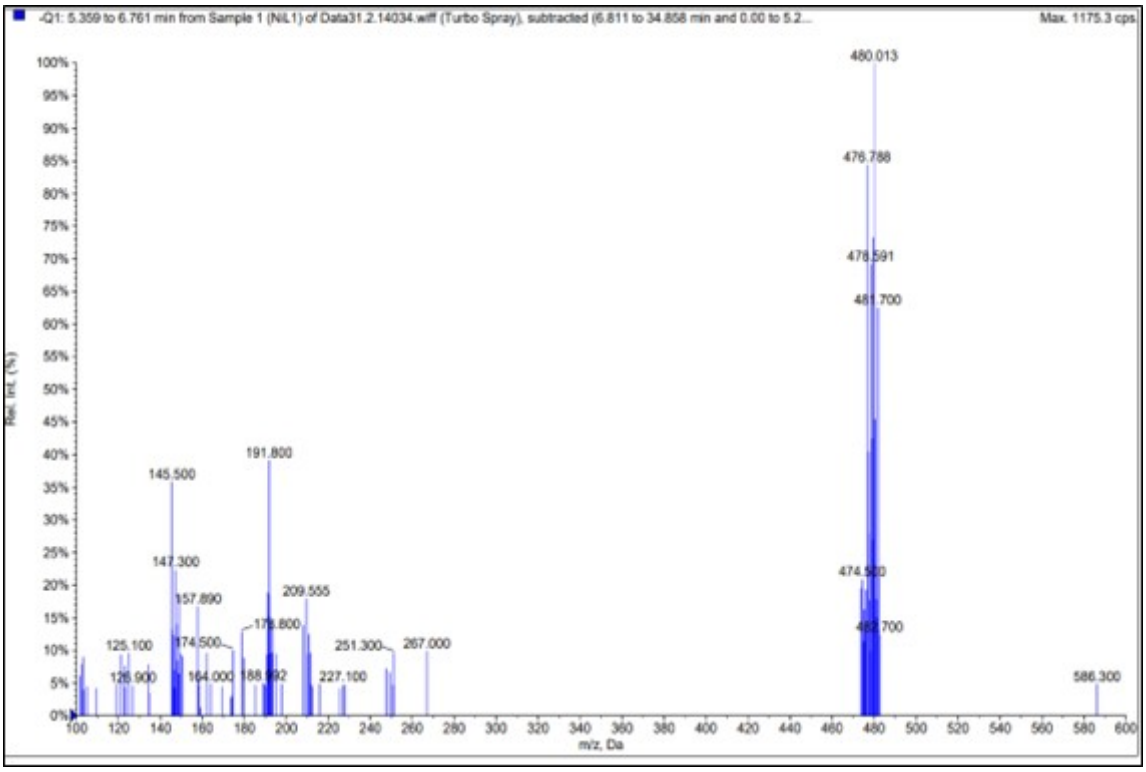

Figure 8. ESI-Mass Spectrometry Analysis of the $[Ni(C_{14}H_{13}NO_2)(OAC)_2(H_2O)_2]$

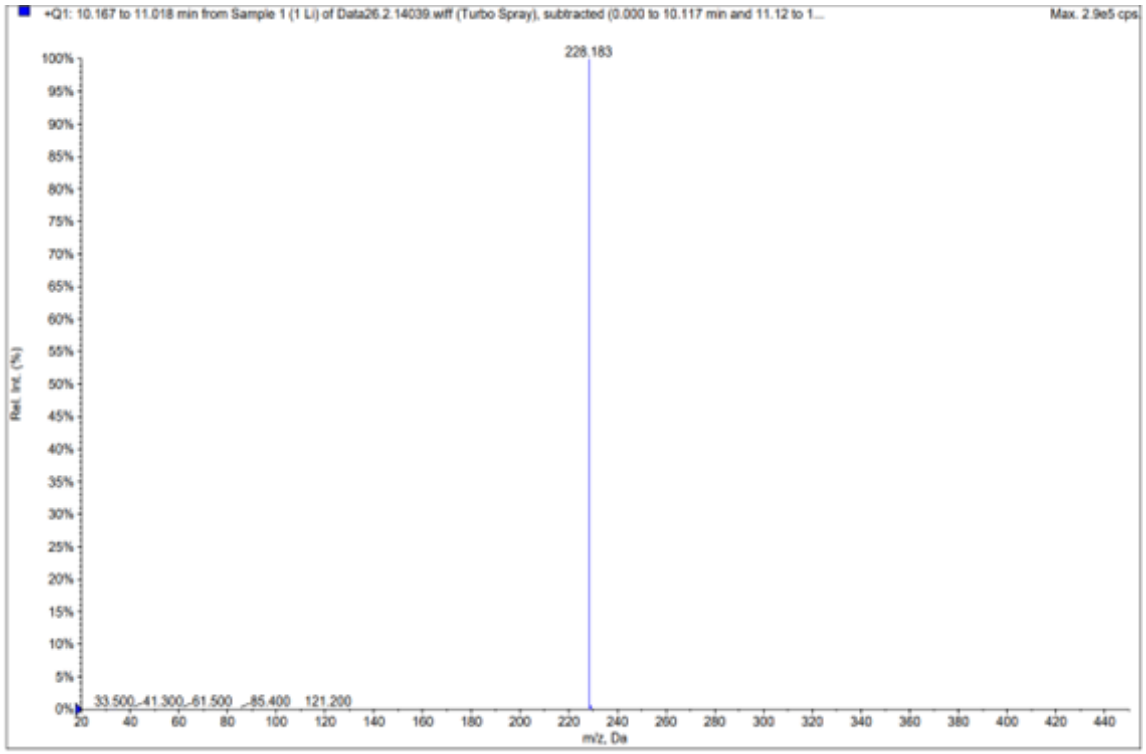

Figure 9. ESI-mass spectrum of the MBZ (ligand)

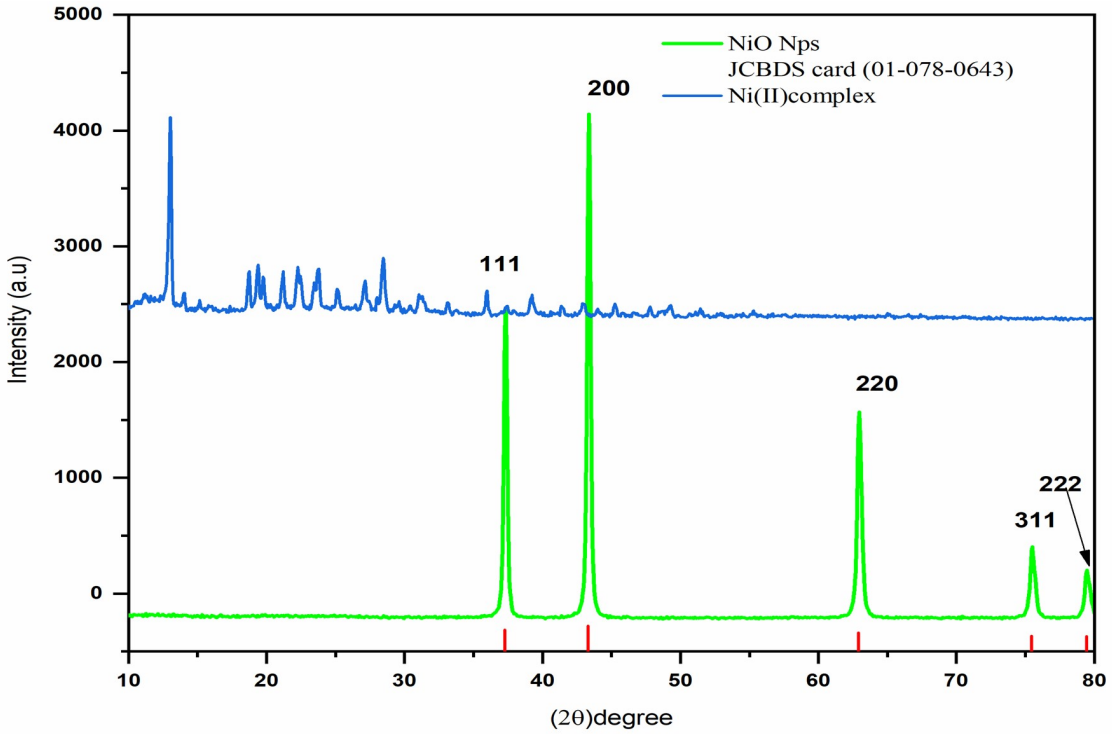

Figure 10. XRD Characterization of the $[Ni(C_{14}H_{13}NO_2)(OAC)_2(H_2O)_2]$ and NiO Nps

Table 5. EDX Characterization of NiO Nanoparticles.

Element	Line	Int.	Error	K	Kr	W%	A%
O	Kα	174.4	5.8187	0.1336	0.1172	19.84	47.60
Ni	Kα	416.7	0.9970	0.8664	0.7601	80.16	52.40
				1.0000	0.8773	100.00	100.00

ing the molecular fragments of a compound. The number of known ions represents the charge ratio. The intensity of the individual peaks indicates the number of ions at each m/z value. The mass spectrometric data provide valuable insights into the fragmentation mechanism of the complex $C_{16}H_{22}NNiO_{11}$. By analyzing the m/z ratios and their relative energies, one can infer the presence and probability of certain fragments, which is important in gaining a better understanding of compounds and their behavior. The mass spectrum shows a peak at 476.788 Da, which corresponds to the molecular ion $[M+H]^+$ with the chemical formula $C_{18}H_{26}NNiO_{10}$ and a molecular weight of 475.10 g/mol. The presence of a Ni isotopic pattern is also evident, with the m/z values including 474.500, 476.788, 478.591, 480.013, 481.700, and 482.700 Da – these peaks may be isotopic patterns of chemically rich Ni.

The m/z ratio of the highest intensity, at 191.800 Da, can be explained by the loss of a nickel-containing fragment, while the peaks at m/z 145.500 and 147.300 Da could indicate further loss of parts of the ligand, which have not been disclosed in the work. The effect at m/z 209.555 Da could indicate a fragment including the nickel atom as well as a segment of the ligand. These peaks could include the molecular ion peak that belongs to the positive ion mode and isotopic peaks. The base peak (100% relative intensity) in Figure 9 appears at m/z 228.207 Da, which corresponds to the molecular ion $[M]^+$ in the solution, 2-[(4-methoxybenzylidene)amino]phenol (chemical formula of $C_{14}H_{13}NO_2$ and molecular weight of 227.258 g/mol). This suggests that the compound is present in the sample. This level is close to the molecular weight of a potential fragment or related compound, suggesting that it could be a large portion of the presented molecule.

3.4 Characterization of NiO Nanoparticles

3.4.1 XRD of the Ni(II) Schiff Base Complex and NiO NPs

XRD is a powerful technique that is often employed for assessing the crystalline structure of materials, including various types of NPs, such as NiO. XRD analysis was conducted herein for further confirmation of the synthesis of the NiO NP phase; its synthesis is supported, as shown in Figure 10. According to the analysis, before calcination, the Ni(II) Schiff base complex shows a crystalline phase, and characteristic peaks corresponding to the crystal lattice of the complex can be observed. No

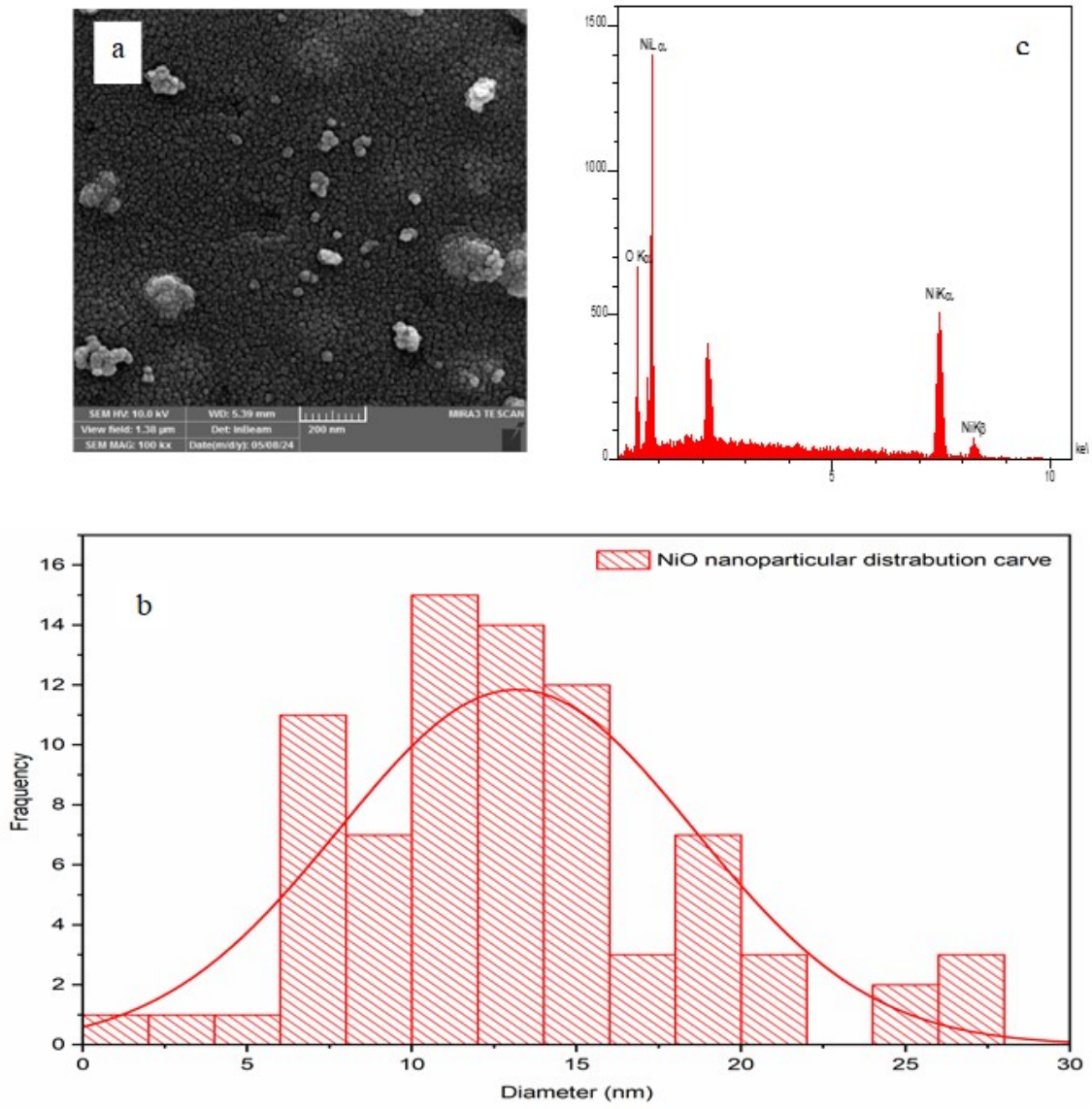

Figure 11. (a) SEM Image, (b) Distribution Curve, and (c) EDX Spectrum of NiO Nanoparticles

peaks corresponding to the NiO phase can be observed in Figure 8 (Khalaji and Das, 2014). After calcination, the presence of additional peaks in the Ni(II) complex pattern compared to NiO may indicate the formation of new crystallographic phases, such as a cubic structure, in which all the diffraction lines correspond to NiO. However 2θ = 37.33°, 43.36°, and 62.94° - were indexed to an ordered structure JCBDS card (01-078-0643) (Ananthi et al., 2023). At the crystalline phase, with all diffraction peaks at (111), (200), (220), (311), and (222), the (D) aveage was estimated to be 26.00 nm according to the Debye–Scherrer equation (Equation 3) and the XRD data:

$$X = \frac{K\lambda}{\beta cos(\theta)} \tag{3}$$

where

- X is the average crystallite size,
- K is the Scherrer constant (typically around 0.9),
- λ is the wavelength of the X-rays (usually 0.154 nm for copper Kα radiation),
- β is the full width at half maximum (FWHM) of the diffraction peak (radians), and
- θ is the Bragg angle.

3.4.2 SEM and EDX Characterization

SEM and EDX spectroscopies were used to characterize the size, shape, and surface composition of the as-synthesized NiO, and the morphological features of as-obtained NiO's samples by microwave irradiation were investigated by SEM as shown in Figure 11. A typical SEM image of the as-synthesized NiO is presented in Figure 11a. The size of the NPs were estimated

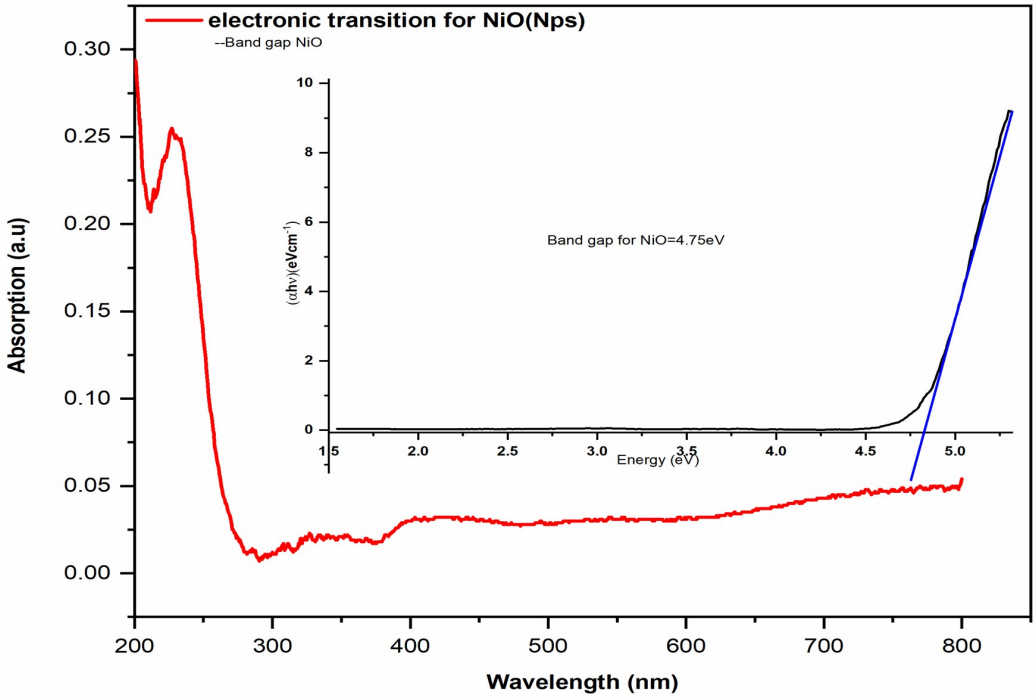

Figure 12. Electronic Spectrum and Bandgap of the NiO NPs

using ImageJ software and the particle size distribution histograms obtained from the images are shown in Figure 11b. Based on the NiO particle sizes, 5-30 nm, with the averaged diameter by 30.1±10.5 nm (Musevi et al., 2016). According to the EDX analysis, the NP elemental composition guaranteed that the EDX spectra. As shown in Figure 11c, the NP had a high weight percentage of nickel and oxygen with a weight percent (wt.%) of 76.02% and 23.98% respectively. In the synthesised NPs, there were no other coexisting elements present as impurities (Pallares-Rusinol et al., 2023). Characterization results demonstrate that the NiO nanoparticles exhibit high crystallinity, uniform morphology, and exceptional phase purity (Bakhsh et al., 2021). Table 5 presents the EDX characterization of the NiO NPs.

3.4.3 Bandgap of NiO Nanoparticles

The bandgap of NiO was show in Figure 12 is an important parameter for understanding its electronic properties. The NiO bandgap has been extensively studied, and experimental measurements have been reported in the literature. It is depicted in and is typically in the range of 3.5 to 4.0 eV, depending on factors such as the crystalline phase, particle size, and synthetic method. The energy gap can be determined via an optical method using Equation 4, where α is the absorption coefficient; A is a constant; Eg is the energy gap; and n can either be $\frac{1}{2}$, for a direct allowed transition, or 2, for an indirect allowed transition (Jubu et al., 2024; Khodov et al., 2023; Supin et al., 2024).

$$\alpha hv = A(hv - Eg) \quad (4)$$

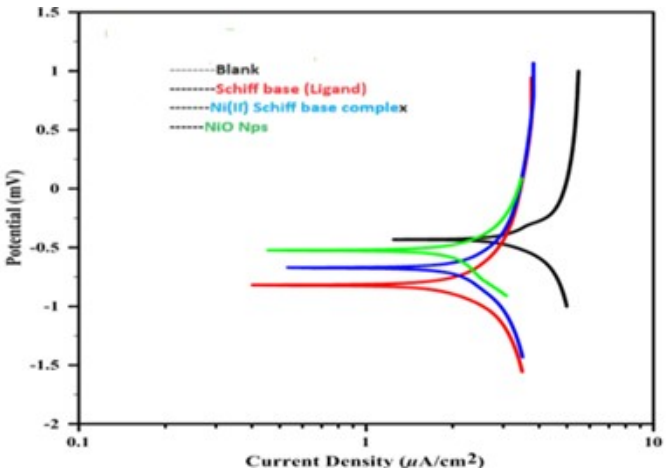

Figure 13. Polarization Curves for the Corrosion Inhibition of the lank,MBZ (Ligand), $[Ni(C_{14}H_{13}NO_2)(OAC)_2(H_2O)_2]$, and NiO Nanoparticles in HCl Solution

3.4.4 Corrosion Inhibition of the MBZ (ligand), $[Ni(C_{14}H_{13}NO_2)(OAC)_2(H_2O)_2]$, and NiO Nanoparticles

Corrosion inhibition is critical for protecting metals from degradation in various environments and involves using substances known as inhibitors to reduce or prevent their corrosion. Inhibitors can be organic, inorganic, or based on complex compounds. The use of a 1 M HCl solution for corrosion studies on mild steel is common in corrosion research. However, other concentrations and types of acid can be used depending on the

Table 6. Corrosion Parameters for the Blank, Ligand (MBZ), $[Ni(MBZ)(OAC)_2(H_2O)_2]$, and NiO Nanoparticles in HCl Solution

Compound	Blank	Schiff Base (Ligand)	Ni(II) Schiff Base Complex	NiO NPs
$-E_{corr}$(mV)	-0.427	-0.774	-0.732	-0.675
i_{corr} (μA/cm^2)	493.9	110.3	82.75	49.88
I_{corr}./r (A/cm^2)	9.87E-4	2.20E-4	1.65E-4	9.97E-5
Resis. (Ω)	70.31	1036	1123	1743
$-\beta$c (mV/Dec)	0.156	0.574	0.380	0.373
Ba (mV/Dec)	0.164	0.486	0.490	0.432
Corr.rate (mm/y)	4.848	1.083	0.812	0.490
IE%	-	78	83	90

Note: E corrosion ($-E_{corr}$), mV; I corrosion (i_{corr}), μA/cm^2; I corrosion per surface area (I corr./r), A/cm^2; polarization resistance (Resis.), Ω; cathodic β Tafel constant ($-\beta$c), mV/decade; anodic β Tafel constant (βa), mV/decade; corrosion rate (Corr. rate), mm/year; and IE% = inhibition efficiency.

needs and constraints of the work. There are several reasons to select 1 M HCl. First, using a standardized concentration of 1 M makes it simple to compare results across different studies or laboratories and also provides a standard basis for rating the corrosion resistance of materials. Second, 1 M HCl is sufficiently aggressive to cause visible corrosion to mild steel after an appropriate amount of time, making it effective for studying the effects of corrosion .In addition, despite being a strong acid, HCl at a concentration of 1 M is practical and safe to use in a regular laboratory environment. Compared to higher HCl concentrations, the lower concentration of 1 M carries less risk to personnel and equipment. Furthermore, the corrosion rate in 1 M HCl is sufficiently high to allow for detailed kinetic studies over a suitable experimental period, which is crucial in elucidating the mechanisms of corrosion and inhibitor effectiveness (Aslam et al., 2020; Laadam et al., 2022). As presented in Table 6, the inhibition efficiency of the NiO NPs is more than that of the $[Ni(MBZ)(OAC)_2(H_2O)_2]$ complex and a ligand (MBZ) .This can be attributed to several factors. Firstly, significant differences exist between the surface-area-to-volume ratio of the NiO NPs, Ni(II) Schiff base complex, and Schiff base ligand. Larger surface areas allow for more coverage of the steel surface, which could enhance the formation of the coating. Therefore, the NPs show enhanced or more substantive adsorption onto the metal surface due to their larger surface area, possibly creating a stronger barrier against corrosive agents. Secondly, the physical barrier created by the NiO NPs significantly helps to protect the surface of the metal as the densified and compact layer of material acts as a constraint to the penetration of species that are corrosive to steel, such as chloride ions and oxygen. NiO is typically insoluble in acidic environments. This property proves invaluable through the formation of a nickel protective layer. The linkage of a Schiff base to a nickel ion makes it simpler for the ligand to donate states to the metal layer, thus ensuring greater success in delivering electrons to the metal surface.

This can provide a better protective barrier that hinders corrosive agents from contacting the steel surface, thus reducing corrosion. The $[Ni(MBZ)(OAC)_2(H_2O)_2]$ complex exhibits the inhibitive performance of both the metal ion and the Schiff base ligand. The nickel ion can contribute to further protection by forming a passive film, and the Schiff base ligand can assist in adsorption and the formation of a corrosion-inhibiting film. The chelation effect stabilizes and strengthens the performance of the inhibitor in the Nickel complex; furthermore, it can adjust the electron distribution and increase the affinity of the inhibitor for the metallic surface (Afshari et al., 2023; Nassar et al., 2015). However, polarization curves are a powerful tool in electrochemical corrosion studies, providing insights into the corrosion behavior of metals via the analysis of their electrochemical reactions under varying potential conditions. In investigating a Schiff base inhibitor, the polarization curves (as shown in Figure 13) exhibit a reduction in both anodic and cathodic currents, indicating a mixed inhibition effect. The corrosion potential may shift slightly, and the corrosion current density (i_{corr}) decreases, reflecting a lower corrosion rate. Similarly, these often show more pronounced effects in polarization studies. The curves might display a significant shift in corrosion potential and a greater reduction in the corrosion current density compared to free Schiff bases due to the formation of a more stable and adherent protective film on the metal surface. Furthermore, polarization studies of NiO coatings or additions to the electrolyte typically show a significant decrease in the corrosion current density, indicating strong passivation and protective behavior. The passive region might be more extended, and the breakdown potential (E_b) might be higher, indicating improved resistance to localized corrosion.

4. CONCLUSIONS

The preparation of NiO NPs from $[Ni(MBZ)(OAC)_2(H_2O)_2]$ involved preparing the Ligand and then complex. Various spectroscopic techniques (FTIR, ^{1}H-NMR, and atomic absorption spectroscopy; and XRD) were used to confirm the formation of the Ni(II) complex and the linking of the ligand, and the NiO NPs were obtained via thermal decomposition. FTIR spectroscopy and XRD revealed a gradual decomposition of the

precursor to produce NiO NPs with high purity and an average particle size of approximately 26 nm, confirming their presence. The calculated particle size in this study is very similar to the grain size obtained from the FESEM and XRD analyses. UV-Vis spectroscopy was used to study the optical bandgap of 4.75 eV, which does indicate a red shift on size reduction. Compared to the Schiff base and Ni(II) complex, this method has also been validated with the obtained size. The method presents a simple and easy approach to producing NiO NPs under controlled parameters for numerous applications. For example, in the areas of corrosion inhibition, catalysis, and sensing, it is possible to tune the material properties for the desired application. We evaluated and modeled the effectiveness of corrosion inhibition by synthesizing and testing three electrode-based corrosion inhibitors, finding that the NiO NPs provide more protection than the Schiff base and Ni(II) complex.

5. ACKNOWLEDGMENT

We would like to thank the "University of Babylon, Iraq", for its generous provision of facilities and support. This research would not have been possible without their involvement.

REFERENCES

Afshari, F., E. R. Ghomi, M. Dinari, and S. Ramakrishna (2023). Recent Advances on the Corrosion Inhibition Behavior of Schiff Base Compounds on Mild Steel in Acidic Media. *ChemistrySelect*, **8**(9); e202203231

Agrawal, P. K. and G. Blunden (2023). Methoxy ^{13}C NMR Chemical Shift as a Molecular Descriptor in the Structural Analysis of Flavonoids and Other Phenolic Compounds. *Natural Product Communications*, **18**(6); 1934578X231171002

Ahmed, A. A. and G. M. Galtima Lemos (2021). Synthesis and Characterization of Ni(II) Complex with Schiff Base Derived from Benzophenone and 2-Aminophenol. *Journal of Chemistry Letters*, **2**(3); 114–119

Ananthi, S., M. Kavitha, A. Balamurugan, E. Ranjith Kumar, G. Magesh, A. F. Abd El-Rehim, and C. Sharmila Rahale (2023). Synthesis, Analysis and Characterization of Camellia Sinensis Mediated Synthesis of NiO Nanoparticles for Ethanol Gas Sensor Applications. *Sensors and Actuators B: Chemical*, **387**; 133742

Ansari, K., M. Quraishi, and A. Singh (2014). Schiff's Base of Pyridyl Substituted Triazoles as New and Effective Corrosion Inhibitors for Mild Steel in Hydrochloric Acid Solution. *Corrosion Science*, **79**; 5–15

Aslam, R., M. Mobin, Huda, I. B. Obot, and A. H. Alamri (2020). Ionic Liquids Derived from α-Amino Acid Ester Salts as Potent Green Corrosion Inhibitors for Mild Steel in 1M HCl. *Journal of Molecular Liquids*, **318**; 113982

Atta, A. M., G. El-Mahdy, and H. A. Al-Lohedan (2013). Corrosion Inhibition Efficiency of Modified Silver Nanoparticles for Carbon Steel in 1 M HCl. *International Journal of Electrochemical Science*, **8**(4); 4873–4885

Atzin-Macedo, C. M., C. Pastor-Ramírez, R. González-Peláez, F. J. Pérez-Flores, S. Hernández-Anzaldo, H. Vazquez-Lima, and Y. Reyes-Ortega (2020). Tautomeric Study of Schiff Bases Derived from O-Dihydroxybenzaldehyde by UV-Vis, IR, ^{1}H NMR, ^{13}C NMR Spectroscopy and Computational Modeling. *ChemistrySelect*, **5**(36); 11120–11126

Bader, A. T., N. A. R. Al-Qasii, and A. M. N. Khaleel (2024). Synthesis and Characterization of CuO and NiO Nanoparticles Derived from Schiff Base Complexes. *Science and Technology Indonesia*, **9**(1); 103–112

Bain, G. A. and J. F. Berry (2008). Diamagnetic Corrections and Pascal's Constants. *Journal of Chemical Education*, **85**(4); 532

Bakhsh, H., J. Buledi, N. Khand, B. Junejo, A. Solangi, A. Mallah, and S. T. Sherazi (2021). NiO Nanostructures Based Functional Non-Enzymatic Electrochemical Sensor for Ultrasensitive Determination of Endosulfan in Vegetables. *Journal of Food Measurement and Characterization*, **15**; 1–10

Boulechfar, C., H. Ferkous, A. Delimi, M. Berredjem, A. Kahlouche, A. Madaci, and A. Errachid (2023). Corrosion Inhibition of Schiff Base and Their Metal Complexes with [Mn(II), Co(II) and Zn(II)]: Experimental and Quantum Chemical Studies. *Journal of Molecular Liquids*, **378**; 121637

Devi, J., S. Kumar, B. Kumar, S. Asija, and A. Kumar (2022). Synthesis, Structural Analysis, in Vitro Antioxidant, Antimicrobial Activity and Molecular Docking Studies of Transition Metal Complexes Derived from Schiff Base Ligands of 4-(Benzyloxy)-2-Hydroxybenzaldehyde. *Research on Chemical Intermediates*, **48**(4); 1541–1576

Ezeorah, C. J., L. C. Ekowo, S. I. Eze, T. Groutso, S. Atiga, S. N. Okafor, and O. C. Okpareke (2022). Synthesis, Characterization, and in Silico Studies of 2-[(E)-(2,5-Dimethoxybenzylidene)Amino]Phenol and 3-[(E)-(2,5-Dimethoxybenzylidene)Amino]Phenol. *Journal of Molecular Structure*, **1270**; 133902

Gönül, I., E. Faki, B. Ay, M. Köse, and S. Serin (2018). Cobalt(II), Nickel(II) and Copper(II) Complexes of a Schiff Base Ligand: Synthesis, Structural Characterization and Luminescence Properties. *Transition Metal Chemistry*, **43**(1); 73–81

Jubu, P. R., E. Danladi, U. Ndeze, O. Adedokun, S. Landi Jr, A. Haider, and F. Yam (2024). Comment About the Use of Unconventional Tauc Plots for Bandgap Energy Determination of Semiconductors Using UV-Vis Spectroscopy. *Results in Optics*, **14**; 100606

Kareem, M. J., A. A. S. Al-Hamdani, V. Y. Jirjees, M. E. Khan, A. W. Allaf, and W. Al Zoubi (2021). Preparation, Spectroscopic Study of Schiff Base Derived from Dopamine and Metal Ni (II), Pd (II), and Pt (IV) Complexes, and Activity Determination as Antioxidants. *Journal of Physical Organic Chemistry*, **34**(3); e4156

Kargar, H., M. Ashfaq, M. Fallah-Mehrjardi, R. Behjatmanesh-

Ardakani, K. S. Munawar, and M. N. Tahir (2022). Synthesis, Crystal Structure, Spectral Characterization, Theoretical and Computational Studies of Ni (II), Cu (II) And Zn (II) Complexes Incorporating Schiff Base Ligand Derived From 4-(Diethylamino) Salicylaldehyde. *Inorganica Chimica Acta*, **536**; 120878

Kargar, H., R. Behjatmanesh-Ardakani, M. Fallah-Mehrjardi, V. Torabi, K. S. Munawar, M. Ashfaq, and M. N. Tahir (2021). Ultrasound-Based Synthesis, SC-XRD, NMR, DFT, HSA f oNew Schiff Bases Derived From 2-Aminopyridine: Experimental and Theoretical Studies. *Journal of Molecular Structure*, **1233**; 130105

Kashyap, S., S. Kumar, K. Ramasamy, S. M. Lim, S. A. A. Shah, H. Om, and B. Narasimhan (2018). Synthesis, Biological Evaluation and Corrosion Inhibition Studies of Transition Metal Complexes of Schiff Base. *Chemistry Central Journal*, **12**(1); 117

Khalaji, A. D. and D. Das (2014). Synthesis and Characterizations of NiO Nanoparticles via Solid-State Thermal Decomposition of Nickel(II) Schiff Base Complexes. *International Nano Letters*, **4**(3); 117

Khodov, I., K. Belov, M. Krestyaninov, V. Sobornova, A. Dyshin, and M. Kiselev (2023). Does DMSO Affect the Conformational Changes of Drug Molecules in Supercritical CO_2 Media? *Journal of Molecular Liquids*, **384**; 122230

Kumar, S., J. Devi, A. Dubey, D. Kumar, D. K. Jindal, S. Asija, and A. Sharma (2023). Co (II), Ni (II), Cu (II) and Zn (II) Complexes of Schiff Base Ligands: Synthesis, Characterization, DFT, *In Vitro* Antimicrobial Activity and Molecular Docking Studies. *Research on Chemical Intermediates*, **49**(3); 939–965

Laadam, G., F. Benhiba, M. El Faydy, A. Titi, A. S. Al-Gorair, M. Alshareef, and A. Zarrouk (2022). Anti-Corrosion Performance of Novel Pyrazole Derivative for Carbon Steel Corrosion in 1 M HCl: Computational and Experimental Studies. *Inorganic Chemistry Communications*, **145**; 109963

Lupascu, G., E. Pahonțu, S. Shova, S. F. Barbuceanu, M. Badea, C. Paraschivescu, and D. Draganescu (2021). Co (II), Cu (II), Mn (II), Ni (II), Pd (II), and Pt (II) Complexes of Bidentate Schiff Base Ligand: Synthesis, Crystal Structure, and Acute Toxicity Evaluation. *Applied Organometallic Chemistry*, **35**(4); e6149

Mamudu, U., M. S. Alnarabiji, L. A. Omeiza, Y. Subramanian, I. A. Alnaser, R. C. Lim, and E.-S. M. Sherif (2024). Biosynthesis of Nickel Oxide Nanocomposite: Experimental and Molecular Modelling of Its Carbon Steel Corrosion Protection in Acidizing Environment and Synergistic Effect Of NAI. *Surface and Coatings Technology*; 130937

Mishra, M., K. Tiwari, P. Mourya, M. Singh, and V. P. Singh (2015). Synthesis, Characterization and Corrosion Inhibition Property of Nickel (II) and Copper (II) Complexes with Some Acylhydrazine Schiff Bases. *Polyhedron*, **89**; 29–38

Mofidabadi, A. H. J., A. Dehghani, G. Bahlakeh, and B. Ramezanzadeh (2024). Combined Clove Extract Bio-Moleculesa and Zinc (II) Ion Synergistic Effects in Steel Corrosion Mitigation in Saline Solution: Electronic (DFT) Modeling, Atomic/Molecular (MC/MD) Simulations, and Corrosion Measurement. *Biomass Conversion and Biorefinery*, **14**(8); 9519–9539

Musevi, S. J., A. Aslani, H. Motahari, and H. Salimi (2016). Offer a Novel Method for Size Appraise of NiO Nanoparticles by PL Analysis: Synthesis by Sonochemical Method. *Journal of Saudi Chemical Society*, **20**(3); 245–252

Nassar, A. M., A. M. Hassan, M. A. Shoeib, and A. N. El kmash (2015). Synthesis, Characterization and Anticorrosion Studies of New Homobimetallic Co(II), Ni(II), Cu(II), And Zn(II) Schiff Base Complexes. *Journal of Bio- and Tribo-Corrosion*, **1**(3); 19

Nassar, M. Y., H. M. Aly, E. A. Abdelrahman, and M. E. Moustafa (2017). Synthesis, Characterization, and Biological Activity of Some Novel Schiff Bases and Their Co(II) and Ni(II) Complexes: a New Route for Co_3O_4 and NiO Nanoparticles for Photocatalytic Degradation of Methylene Blue Dye. *Journal of Molecular Structure*, **1143**; 462–471

Öz, S., P. A. Bozkurt, S. B. Sopacı, N. Acar, and O. Atakol (2022). Synthesis And Characterization of NiO Nanoparticles by Using Thermal Decompositions of Ni (II)-ONO and ONNO Type Schiff Base Complexes. *Süleyman Demirel Üniversitesi Fen Bilimleri Enstitüsü Dergisi*, **26**(2); 200–210

Pallares-Rusinol, A., M. Bernuz, S. L. Moura, C. Fernández-Senac, R. Rossi, M. M., and M. I. Pividori (2023). *Advances in Clinical Chemistry*, volume 112, chapter Chapter Two - Advances in Exosome Analysis. Elsevier, pages 69–117

Parsaee, Z., K. Mohammadi, M. Ghahramaninezhad, and B. Hosseinzadeh (2016). A Novel Nano-Sized Binuclear Nickel(II) Schiff Base Complex as a Precursor for NiO Nanoparticles: Synthesis, Characterization, DFT Study and Antibacterial Activity. *New Journal of Chemistry*, **40**(12); 10569–10583

Platzer, G., M. Mayer, A. Beier, S. Brüschweiler, J. E. Fuchs, H. Engelhardt, and R. Lichtenecker (2020). PI By NMR: Probing $CH^{-}\pi$ Interactions in Protein-Ligand Complexes by NMR Spectroscopy. *Angewandte Chemie*, **132**(35); 14971–14978

Prabhakar, U. P. S., G. Periyasami, and P. Karthikeyan (2024). Nanostructured Metal Oxides Synthesized via Simple Thermal Decomposition Of Co(II), Ni(II), Cu(II), and Zn(II) Schiff Base Complexes: Characterization and Antimicrobial Activity. *Inorganic Chemistry Communications*, **159**; 111796

Quevedo, R. (2020). ^{1}H and ^{13}C-NMR Spectroscopic Study of Intermolecular Interactions between Tyrosine-Derived Azacyclophanes and Aromatic Rings. *Journal of Molecular Structure*, **1207**; 127777

Raczuk, E., B. Dmochowska, J. Samaszko-Fiertek, and J. Madaj (2022). Different Schiff Bases-Structure, Importance and Classification. *Molecules*, **27**(3); 787

Rakhtshah, J. (2022). A Comprehensive Review on the Synthesis, Characterization, and Catalytic Application of Transition-Metal Schiff-Base Complexes Immobilized on Magnetic Fe_3O_4 Nanoparticles. *Coordination Chemistry Reviews*, **467**;

214614
Ramachandran, H., M. M. Jahanara, N. M. Nair, and P. Swaminathan (2020). Metal Oxide Heterojunctions Using a Printable Nickel Oxide Ink. *RSC Advances*, **10**(7); 3951–3959
Sharma, S., S. Chauhan, Anushree, and M. Sindhu (2022). Synthesis, Spectral Studies and Antimicrobial Activities of *P*-Anisalidene-O-Aminophenol and Their Metal Complexes. *Environment and Ecology*, **40**(4C); 2540–2547
Silverstein, R. M., F. X. Webster, and D. J. Kiemle (2005). *Spectrometric Identification of Organic Compounds*. Wiley
Streicher, M. (2018). *Application of Phase Imaging at High Field - MR Thermometry at 7 Tesla*. Ph.D. thesis, der Universitat Leipzig
Supin, K., P. Namboothiri, and M. Vasundhara (2024). Complex Magnetic Behaviour and Photocatalytic Response in Narrowed Band Gap NiO Nanoparticles Synthesized by Novel *Lepidagathis ananthapuramensis* Leaf Extract. *Materials Science and Engineering: B*, **300**; 117126
Wadhwani, P. M., D. G. Ladha, V. K. Panchal, and N. K. Shah (2015). Enhanced Corrosion Inhibitive Effect of p-Methoxybenzylidene-4, 4'-Dimorpholine Assembled on Nickel Oxide Nanoparticles for Mild Steel in Acid Medium. *RSC Advances*, **5**(10); 7098–7111

